Abstract

Ever since 1885, when Lord Rayleigh first predicted the existence of waves that travel along a free surface, observations interpreted to be surface waves have been remarkably useful for helping determine Earth structure and earthquake source properties. Yet despite the theory for both Rayleigh and Love waves being well accepted, and the theoretical predictions accurately matching observations, the observation of their quantifiable decay with depth has never been measured in the Earths crust. The primary difficulty of confirming this decay of motion with depth is that nearly all seismometers are placed at or near the Earths surface, or in isolated borehole installations. In this work, we address this gap in observations by making direct observations of both Rayleigh-wave and Love-wave eigenfunction amplitudes over a range of depths, using data collected at the three-dimensional Homestake Array for a suite of nearby mine blasts. Observations of amplitudes over a range of frequencies from 0.4-1.2 Hz are consistent with theoretical eigenfunction predictions, with clear exponential decay of amplitudes with depth, and a reversal in sign of the radial-component Rayleigh-wave eigenfunction at large depths, as predicted for fundamental-mode Rayleigh waves. Minor discrepancies between the observed eigenfunctions and those predicted using estimates of the local velocity structure suggest that the observed eigenfunctions could be used to improve the velocity model. Our results confirm that both Rayleigh and Love waves have the depth dependence that they have long been assumed to have. While this result is not unexpected, it provides new observational evidence that classical seismological surface-wave theory is indeed relevant and can be used to accurately infer properties of Earth structure and earthquake sources.

Direct Observations of Surface-Wave Eigenfunctions at the Homestake 3D Array

Patrick Meyers[1], Daniel C. Bowden[2], Tanner Prestegard[1], Victor C. Tsai[2], Vuk Mandic[1], Gary Pavlis[3], and Ross Caton[3]

[1]School of Physics and Astronomy, University of Minnesota, Minneapolis, Minnesota 55455, USA
[2]Seismological Laboratory, California Institute of Technology, Pasadena, CA 91125, USA
[3]Department of Geological Sciences, Indiana University, Bloomington, IN 47405, USA

June 1, 2018

1 Introduction

The existence of surface waves has been well predicted and described since at least 1885 by Lord Rayleigh. Specifically, the interaction of compression (P) and shear (S) waves with a free surface will set up either Rayleigh or Love waves along that surface, with propagation velocities and amplitudes that depend on subsurface properties in a predictable manner. These have been observed and used in countless studies in the Earth sciences, for example to constrain crustal properties from surface wave dispersion (e.g., Dziewonski and Anderson, 1981; Shapiro et al., 2005) or ellipticity (e.g., Nakamura, 1989; Lin et al., 2008), to image and understand earthquake source processes (e.g., Duputel et al., 2012)Kanamori, and to better understand the strength of shaking that may occur in future earthquakes (e.g., Kawase and Aki, 1989).

The existence of surface waves is well accepted in geophysics literature. However, perhaps what is the most defining characteristic of these surface waves, that they decay in amplitude in some exponential manner as a function depth, has never been directly demonstrated for the Earths crust. This decay in amplitude is described by the eigenfunctions that result from solving the equations of motion REF, but more than mathematical constructs, the actual particle motion amplitudes should exactly match these expectations. Most of our seismic observations are constrained to the Earths surface on a (relatively speaking) 2D plane, and even locations where borehole instruments were available, sensors

have been either too sparsely spaced or at least the direct observation of surface wave eigenfunctions have not been demonstrated.

In this paper, we confirm that observations of surface wave amplitudes as a function of depth match expectations. These observations are collected from an array of instruments in at the Sanford Research Labartory, previously the Homestake Gold Mine, in South Dakota, U. S. MandicSRL. An array of 24 broadband instruments (15 underground and 9 above ground) were deployed in a 3D array geometry in the otherwise mostly abandoned shafts of the mine, covering a volume roughly 1500m in depth and lateral width (see Mandic for a map Perhaps we should include a 3D / zoomed in version?). Blasts from a nearby mine, on average roughly XXkm away, provide a source of seismic excitations used for our observations of surface wave amplitude as a function of depth, in the frequency range of 0.4 to 1.2 Hz. These observations are compared to predictions of both Rayleigh and Love wave eigenfunctions from two different approaches: by describing the eigenfunctions with a relatively simple bi-exponential model that would perfectly describe the decay with depth for halfspace or power-law velocity models (Tsai and Atiganyanun, 2014), and by constraining a 1D velocity profile from ambient noise cross correlations and then numerically predicting eigenfunctions. As will be shown, the classic descriptions of surface waves eigenfunctions accurately describes the observations.

2 Methods

2.1 Observational Methods

try to make less mathematical. if needed move math to an appendix
do we want to include love-wave information?

We use transient seismic events to measure the surface-wave eigenfunctions. ([text from Gary/Ross on how picking is done, direction/blast time is estimated. Maybe plot of transient events]).

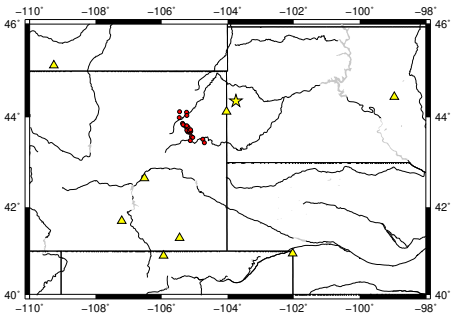

Figure 1: fill me

For each transient event, we rotate from East West/North South coordinates to radial and transverse coordinates. We then plot the waveform and a frequency-time map of the phase delay between the radial and vertical channels for each event for several surface stations. We identify times and frequencies when the radial-to-vertical phase is consistent with retrograde motion, which indicates that surface-waves are the dominant component of the seismic field. We define the radial-to-vertical phase using the cross-correlation of radial and vertical channels

$$\phi_{RV}(f,t) = \arctan\left[\frac{\mathrm{Im}\left(\tilde{R}^*(f,t)\times\tilde{V}(f,t)\right)}{\mathrm{Re}\left(\tilde{R}^*(f,t)\times\tilde{V}(f,t)\right)}\right]. \quad (1)$$

$\tilde{R}(f,t)$ indicates the Fourier transform of the radial data at frequency f for the time segment starting at time t. $\tilde{V}(f,t)$ indicates the same for the vertical channel. The asterisk indicates complex conjugation, while "Im" indicates the imaginary part of the cross-correlation and "Re" indicates the real part. ([add figure with trace and ft-map? and/or location of mine blasts used? or table of dates, etc.?]).

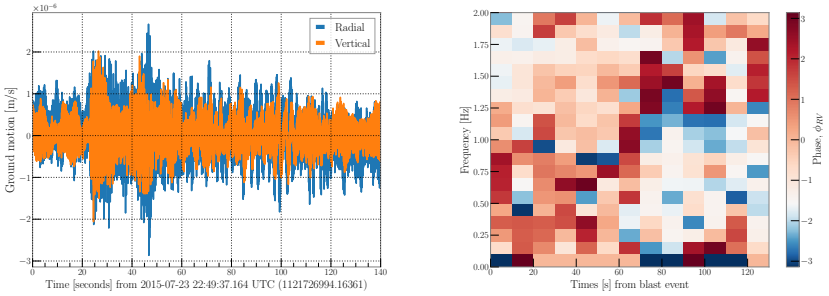

Figure 2: Left: The trace for the YATES surface station vertical and radial channels for an event July 23rd, 2015. Right: The vertical-to-radial phase, ϕ_{RZ}, for the same YATES station over the same time frame. We use 10 s discrete Fourier transforms. The colorbar is normalized such that white indicates a phase of $-\pi/2$, which corresponds to retrograde motion. We see strong evidence for retrograde motion between $70-140$ s and $0.2-1.2$ Hz. make ticks and labels larger.

We use 28 mine blasts observed by the Homestake seismometer array during July 2015. We have used the above prescription to identify which parts of the waveforms are dominated by surface waves. For each blast, we calculate as many discrete Fourier transforms of length 10 s as possible for each seismometer in the array. This leaves us with 0.1 Hz frequency resolution, and we restrict our observations to the frequency band from $0.4-1.2$ Hz for both the radial and

the vertical channels because this is the region of frequency space where most of the surface-wave power appears to be concentrated for these blasts. We refer to the radial data point at frequency, f, and time, t, in seismometer, i, located at depth, z_i, as $\tilde{R}_i(f,t;z_i)$, and the corresponding vertical data point as $\tilde{V}_i(f,t;z_i)$.

We are attempting to observe Rayleigh waves and so we only consider the part of the radial measurement that is consistent with retrograde motion. This means that we perform a projection of our data onto the phase angle consistent with retrograde motion phrasing a bit awkward...

$$\tilde{\mathcal{R}}_i(f,t;z_i) = -|\tilde{R}_i(f,t;z_i)| \times \text{Im } e^{i\phi_{RV}}. \tag{2}$$

In the above expression, vertical lines indicate modulus, and we use the minus sign to impose the condition that measurements consistent with retrograde motion are positive, while those consistent with prograde motion are negative. $\tilde{\mathcal{R}}_i(f,t;z_i)$ is now a real-valued quantity.

We then normalize each data point by the average over radial surface station measurements of the corresponding time and frequency. That is

$$\hat{r}_i(f,t;z_i) = \frac{\tilde{\mathcal{R}}_i(f,t;z_i)}{\text{mean}\left[\{\tilde{\mathcal{R}}_j(f,t;0) \text{ for } j \text{ where } z_j = 0\}\right]} \tag{3}$$

$$\hat{v}_i(f,t;z_i) = \frac{|\tilde{V}_i(f,t;z_i)|}{\text{mean}\left[\{\tilde{\mathcal{R}}_j(f,t;0) \text{ for } j \text{ where } z_j = 0\}\right]} \tag{4}$$

In the above expressions, j runs over all stations positioned on the surface, and the minus sign on the vertical component is taken to be consistent with the convention in Haney and Tsai (2015). We remove measurements where $\hat{r}_i(f,t;z_i)$ and $\hat{v}_i(f,t;z_i)$ are greater than 1.5, as values this large indicate outliers whose amplitudes are much larger than the typical amplitude seen across the surface stations. This removes 15% of the individual data pixels.

Finally, we take the mean and variance across all times at each depth and each frequency. We indicate this with

$$\hat{\bar{r}}(f,z) = \frac{1}{N_{t,z}} \sum_{i \text{ for } z_i = z} \sum_t \hat{r}_i(f,z_i;t) \tag{5}$$

$$\sigma_r^2(f,z) = \frac{1}{N_{t,z}} \sum_{i \text{ for } z_i = z} \sum_t \left(\hat{r}_i(f,z_i;t) - \hat{\bar{r}}(f,z)\right)^2, \tag{6}$$

where $N_{t,z}$ indicates the total number of measurements across times and stations at depth z.

In Figure 2 we show the distribution at 1 Hz of the $r_i(1,t;z_i)$ and $v_i(1,t;z_i)$ as a function of depth with the violin plots, while the means, $\hat{\bar{r}}(1;z)$ and $\hat{\bar{v}}(1;z)$ are indicated with orange points. The median across depths and times, as opposed to the mean, is shown in red. The black bars indicate the 16th and 84th percentiles of the distributions shown in blue.

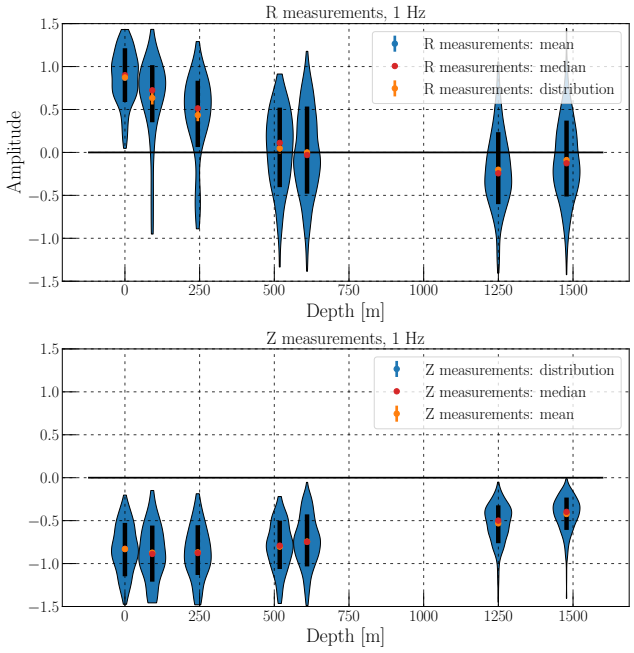

Figure 3: Top: ditribution of radial measurements shown by violin plot. Red and orange points indicate the median and mean of the distribution respectively. Bottom: the same, except for the vertical measurements.maybe move this plot to results section?

2.2 Markov Chain Monte Carlo Estimation of Model Parameters

(need to motivate bi-exponential model properly.) The plots in Figure 3 show a distinctive shape that can be fit by a bi-exponential model. In Haney and Tsai (2015) the authors construct a model for the fundamental R-wave eigenfunction based on a power-law velocity depth profile for S-waves. They fit a bi-exponential model to the R-wave eigenfunction for many different theoretical power-law velocity depth profiles and Poisson ratios and calculate the mean and standard deviation of the parameters in those fits. For this model, the parameters of the bi-exponential model are independent of frequency, althought this need not necessarily be trueadd a source for this statement?.

We use our measurements to estimate the parameters in the bi-exponential fits to the radial and vertical data points. We use m_R and m_V to refer to the bi-exponential models for the radial and vertical eigenfunctions, and these models depend on a set of intrinsic model parameters, $\vec{\theta}$, the depth, z, and the

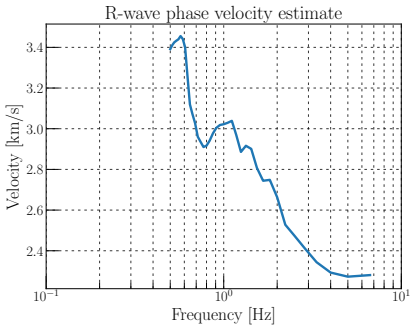

Figure 4: Estimate of phase velocity as a function of frequency obtained from ambient noise correlations at the 3D Homestake seismometer array. not sure how else to cite this...Daniel is it possible to cite Daniel's thesis? Feel free to add comments on updates to plot itself as needed.

frequency, f. We define the m_R and m_V as

$$m_R(f, z; \vec{\theta}) = \left(e^{-2\pi f z \frac{a_1}{c_R(f)}} + c_2 e^{-2\pi f z \frac{a_2}{c_R(f)}}\right) \times \frac{1}{1 + c_2} \tag{7}$$

$$m_V(f, z; \vec{\theta}) = \left(e^{-2\pi f z \frac{a_3}{c_R(f)}} + c_4 e^{-2\pi f z \frac{a_4}{c_R(f)}}\right) \times \frac{N_{vh}}{1 + c_4}. \tag{8}$$

These functions can be compared to r_1 and r_1 in Haney and Tsai (2015). Below, we estimate the parameters in the bi-exponential model,

$$\vec{\theta} = (N_{vh}, c_2, c_4, a_1, a_2, a_3, a_4),$$

using the data, $\hat{\bar{v}}(f, z)$ and $\hat{\bar{r}}(f, z)$. The assumption that the c's and the a's do not change with frequency is intrinsic to the theoretical model outlined in Haney and Tsai (2015) and could, in principle, be relaxed.

this paragraph may be better in previous section The phase velocity dispersion curve for R-waves, $c_R(f)$, is estimated using ambient noise correlations. A plot of $c_R(f)$ is shown in Figure 4.

We use the `MultiNest` package Feroz et al. (2009) to perform a Markov chain monte carlo (MCMC) analysis to estimate the parameters, $\vec{\theta}$. `MultiNest` is commonly used in the astrophysics community, is designed to efficiently sample multimodal distributions and large parameter spaces, and offers robust Bayesian evidence estimates. The posterior probability distribution we use `MultiNest` to explore is given by

$$p(\vec{\theta}|\{\hat{\bar{r}}, \hat{\bar{v}}\}) = \frac{p(\{\hat{\bar{r}}, \hat{\bar{v}}\}|\vec{\theta})p(\vec{\theta})}{\int d\vec{\theta}\, p(\{\hat{\bar{r}}, \hat{\bar{v}}\}|\vec{\theta})p(\vec{\theta})}. \tag{9}$$

The likelihood function, $p(\{\hat{\vec{r}}, \hat{\vec{v}}\}|\vec{\theta})$, is taken to be a Gaussian

$$\ln p(\{\hat{\vec{r}}, \hat{\vec{v}}\}|\vec{\theta}) = -\frac{1}{2}\sum_f \sum_z \left(\frac{\left[\hat{\vec{r}}(f,z) - m_R(f,z;\vec{\theta})\right]^2}{\sigma_r^2(f,z)} + \frac{\left[\hat{\vec{v}}(f,z) - m_V(f,z;\vec{\theta})\right]^2}{\sigma_v^2(f,z)} \right). \tag{10}$$

We assume that the prior probability distribution, $p(\vec{\theta})$, can be split into the product of independent Gaussian prior probability distributions on each individual parameter. We use Haney and Tsai (2015) to inform the Gaussian prior probability distributions. The definition of our parameters differ slightly from those in Haney and Tsai (2015), but we can generate prior information on each parameter using some combination of information from that manuscript. We also widen the uncertainty on those parameters enough to allow for sufficient exploration of the parameter space, given that our situation is likely different from the theoretical one considered in Haney and Tsai (2015).

2.3 Ambient Noise Cross Correlation and Velocity Model

We can also estimate what the eigenfunctions may be for a more realistic velocity model, following methodology that is now relatively commonly used to recover subsurface velocity estimates. This is intended to serve as a completely independent check, and so we focus on ambient noise cross correlations rather than the mine-blast data used above. Ambient noise cross-correlations are collected between each station using one year's worth of data, from June 2015 to June 2016. Standard methods of time-domain normalization with a XX second window and spectral whitening (i.e., Bensen et al., 2007) are used to reduce nonstationary signals in the ambient noise. We note, however, that each of a stations 3 components (vertical, N-S and E-W) are treated with an identical time-domain and frequency-domain envelope derived from the average of the 3 components envelopes. In this way, even though a given station pair has produced a noise correlation function for the North-North and East-East components of motion, these can be safely rotated into the radial and transverse components appropriate to the azimuth between those two stations (Lin et al., 2008; Muir and Tsai, 2017).

Dispersion curves are estimated by passing narrow-bandpass filters over the noise correlation functions, using the automated FTAN package (as described by Levshin and Ritzwoller (2001)), for the frequency range of XX to XX Hz, for fundamental group and phase velocities of both Rayleigh and Love waves (figure XX). A starting velocity model is estimated using the relatively course US-wide model of Schmandt et al. (2015) below 3km depth and the smoothly varying very-hard rock profile of Boore and Joyner (1997). The computer package Computer Programs in Seismology (CPS) by Herrmann (2013) is used to invert for a velocity model, using 12 iterations of estimating misfit between predicted and observed dispersion curves and updating the 1D velocity model accordingly. The resulting velocity model is undoubtedly less well resolved below about 1km, but nevertheless this provides a reasonable estimate of seismic

velocities in the region, and has been estimated using only techniques standard in the literature.

This new 1D profile is then used to predict the corresponding eigenfunctions, again using CPS. In fact, solving the eigenvalue problem to estimate sensitivity kernels was a necessary step for each of the 12 iterations of our inversion, done internally in CPS, but we are primarily interested here in the final set of eigenfunctions produced. These eigenfunctions compare well in the range etc. compare and continue.

3 Results: Observations and Model Estimates

The results of the parameter estimation, along with the prior information on each parameter, is summarized in Figures 5 and 6 and Table 1.

Figure 5 shows that the model fits the data reasonably well across all frequencies used in the analysis. Figure 6 shows that there is very little difference between the prior and posterior distributions, which implies that the measurements generally agree with the theoretical predictions. expand this discussion

These measurements represent the first explicit estimate of the depth dependence of the R-wave eigenfunctions using a three-dimensional seismometer array.

Parameter	Mean	Error	Prior Mean	Prior Error
c_2	-0.76	0.06	-0.8	0.1
a_1	0.86	0.06	0.85	0.1
a_2	0.63	0.06	0.7	0.1
c_4	-0.69	0.07	-0.74	0.1
a_3	0.49	0.06	0.7	0.4
a_4	0.81	0.1	0.8	0.2
N_{vh}	-0.68	0.02	-0.6	0.2

Table 1: values in table need to be updated Results for R-wave eigenfunction parameter estimation. We show estimates and uncertainty for the parameters from the 1-dimensional marginalized posterior distribution on each parameter. We also show the mean and standard deviation of the Gaussian prior probability distribution used for each parameter.

4 Conclusions

fix references for BSSA submission. (alphabetical by author citations are [Author, year])

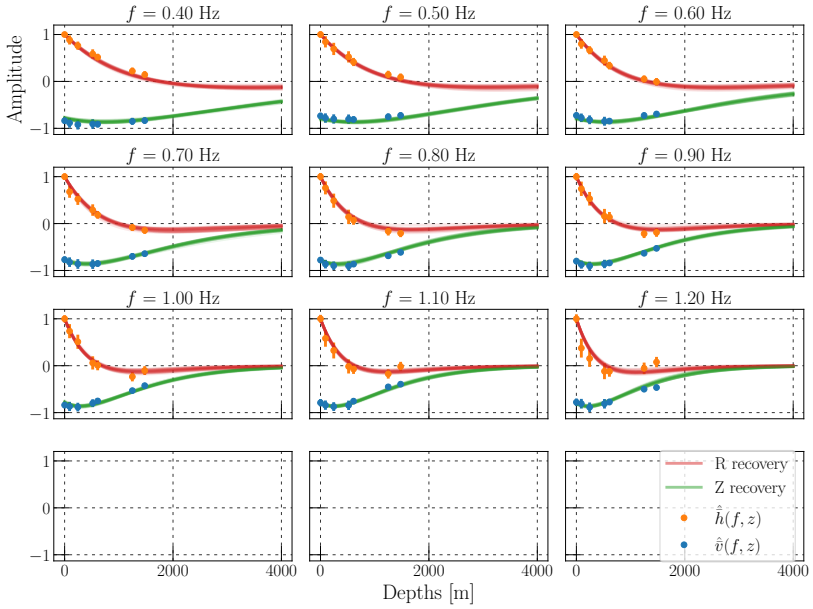

Figure 5: Rayleigh-wave parameter estimation fits for all of the data used. The red and green curves are examples of the bi-exponential models evaluated at parameters whose values are generated with random draws from the posteriors presented in Figure 6. The width of those lines is proportional to the range of values at each depth one might expect the R-wave eigenfunction to take given the parameter estimation we have performed and the model we have used. The orange points are the data supplied to the sampler. That is, the orange points correspond to $\hat{\hat{r}}(f,z)$ and the blue points correspond to $\hat{\hat{v}}(f,z)$.

References

Bensen, G. D., Ritzwoller, M. H., Barmin, M. P., Levshin, a. L., Lin, F., Moschetti, M. P., Shapiro, N. M., and Yang, Y. (2007). Processing seismic ambient noise data to obtain reliable broad-band surface wave dispersion measurements. *Geophysical Journal International*, 169(3):1239–1260.

Boore, D. M. and Joyner, W. B. (1997). Site amplifications for generic rock sites. *Bulletin of the Seismological Society of America*, 87(2):327–341.

Duputel, Z., Rivera, L., Kanamori, H., and Hayes, G. (2012). W phase source inversion for moderate to large earthquakes (1990-2010). *Geophysical Journal International*, 189:1125–1147.

Dziewonski, A. M. and Anderson, D. L. (1981). Preliminary reference Earth model *. *Physics of the Earth and Planetary Interiors*, 25:297–356.

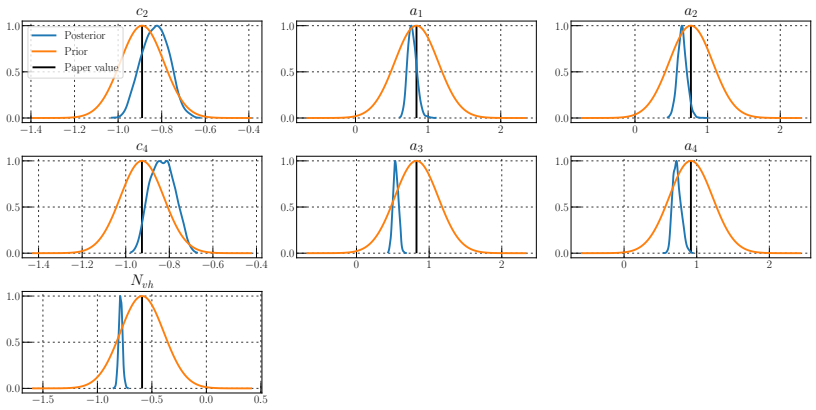

Figure 6: fill me.

Feroz, F., Hobson, M. P., and Bridges, M. (2009). MultiNest: an efficient and robust Bayesian inference tool for cosmology and particle physics. *Monthly Notices of the Royal Astronomical Society*, 398(4):1601–1614.

Haney, M. M. and Tsai, V. C. (2015). Nonperturbational surface-wave inversion: A Dix-type relation for surface waves. *GEOPHYSICS*, 80(6):EN167–EN177.

Herrmann, R. B. (2013). Computer Programs in Seismology: An Evolving Tool for Instruction and Research. *Seismological Research Letters*, 84(6):1081–1088.

Kawase, H. and Aki, K. (1989). A study on the response of a soft basin for incident S, P, and Rayleigh waves with special reference to the long duration observed in Mexico City. *Bulletin of the Seismological Society of America*, 79(5):1361–1382.

Levshin, A. L. and Ritzwoller, M. H. (2001). Automated Detection, Extraction, and Measurement of Regional Surface Waves BT - Monitoring the Comprehensive Nuclear-Test-Ban Treaty: Surface Waves. *Monitoring the Comprehensive Nuclear-Test-Ban Treaty: Surface Waves*, 158(Chapter 11):1531–1545.

Lin, F.-C., Moschetti, M. P., and Ritzwoller, M. H. (2008). Surface wave tomography of the western United States from ambient seismic noise: Rayleigh and Love wave phase velocity maps. *Geophysical Journal International*, 173(1):281–298.

Muir, J. B. and Tsai, V. C. (2017). Rayleigh-Wave H / V via Noise Cross Correlation in Southern California. *Bull. Seism. Soc. Am.*, 107(5):2021–2027.

Nakamura, Y. (1989). A method for dynamic characteristics estimation of subsurface using microtremor on the ground surface. *QR Railway Tech. Res. Inst.*, 30(1):25–33.

Schmandt, B., Lin, F. C., and Karlstrom, K. E. (2015). Distinct crustal isostasy trends east and west of the Rocky Mountain Front. *Geophysical Research Letters*, 42(23):10290–10298.

Shapiro, N. M., Campillo, M., Stehly, L., and Ritzwoller, M. H. (2005). High-resolution surface-wave tomography from ambient seismic noise. *Science (New York, N.Y.)*, 307(5715):1615–8.

Tsai, V. and Atiganyanun, S. (2014). Green's Functions for Surface Waves in a Generic Velocity Structure. *Bulletin of Seismological Society of America*, 104(5):2573–2578.